coatings

MDPI

Article

Tribological Comparison of Coatings Produced by PVD Sputtering for Application on Combustion Piston Rings

Ney Francisco Ferreira [1,2,*], Filipe Fernandes [2,3,4,*], Patric Daniel Neis [1], Jean Carlos Poletto [1,5], Talha Bin Yaqub [2,6], Albano Cavaleiro [2,4], Luis Vilhena [2] and Amilcar Ramalho [2]

1 Laboratory of Tribology, Federal University of Rio Grande do Sul, Osvaldo Aranha, 99, Porto Alegre 90035-190, RS, Brazil
2 University of Coimbra, CEMMPRE, ARISE, Department of Mechanical Engineering, Rua Luís Reis Santos, 3030-788 Coimbra, Portugal
3 CIDEM, ISEP, Polytechnic of Porto, Rua Dr. António Bernardino de Almeida, 4249-015 Porto, Portugal
4 IPN-LED & MAT-Instituto Pedro Nunes, Laboratory of Tests, Wear and Materials, Rua Pedro Nunes, 3030-199 Coimbra, Portugal
5 Soete Laboratory, Ghent University, Technologiepark Zwijnaarde 46, 9000 Gent, Belgium
6 Laboratory for Tribology and Interface Nanotechnology, University of Ljubljana, Bogišićeva 8, 1000 Ljubljana, Slovenia
* Correspondence: ney.ferreira@ufrgs.br (N.F.F.); filipe.fernandes@dem.uc.pt (F.F.)

Abstract: This article compares the tribological performance of coatings produced by PVD sputtering. Transition metal dichalcogenide (TMD) coatings doped with carbon (WSC and MoSeC) and nitrogen (WSN and MoSeN) and a conventional diamond-like carbon (DLC) coating are compared. The tribological evaluation was oriented towards the use of coatings on piston rings. Block-on-ring tests in a condition lubricated with an additive-free polyalphaolefin (PAO 8) and at temperatures of 30, 60, and 100 °C were carried out to evaluate the coatings in boundary lubrication conditions. A load scanner test was used to evaluate dry friction and scuffing propensity. In addition to WSN, all other TMD coatings (WSC, MoSeC, and MoSeN) exhibited lower friction than DLC in dry and lubricated conditions. The study reveals that WSC, among TMD coatings, offers promising results, with significantly lower friction levels than DLC, while demonstrating reduced wear and a lower risk of metal adhesion. These findings suggest that WSC may be a viable alternative to DLC in piston rings, with potential benefits for reducing fuel consumption and increasing engine durability.

Keywords: PVD sputtering; TMD coating; DLC coating; mixed lubrication; piston ring

check for updates

Citation: Ferreira, N.F.; Fernandes, F.; Neis, P.D.; Poletto, J.C.; Yaqub, T.B.; Cavaleiro, A.; Vilhena, L.; Ramalho, A. Tribological Comparison of Coatings Produced by PVD Sputtering for Application on Combustion Piston Rings. *Coatings* **2024**, *14*, 1109. https://doi.org/10.3390/coatings14091109

Academic Editor: Chuen-Lin Tien

Received: 24 July 2024
Revised: 20 August 2024
Accepted: 24 August 2024
Published: 2 September 2024

Copyright: © 2024 by the authors. Licensee MDPI, Basel, Switzerland. This article is an open access article distributed under the terms and conditions of the Creative Commons Attribution (CC BY) license (https://creativecommons.org/licenses/by/4.0/).

1. Introduction

Until the mid-1960s, machine design was based solely on functionality, neglecting aspects related to friction and wear. This resulted in technological backwardness, unnecessary energy expenditure, and component replacement. Only with the report of the Committee of the British Department of Education [1] were the economic aspects related to friction and wear of materials analyzed; this analysis led to significant advances in mechanical design. Following the British example, governmental studies in countries such as Germany, the United States, Canada, and Japan served as a basis for accelerating this process globally [2,3].

In more recent studies, the research group led by Holmberg [4] estimated the impact of friction and wear on energy consumption, economic expenditure, and CO_2 emissions from passenger cars, trucks, and buses [5]; paper machines [6]; and the mining industry [7]. The conclusions were that approximately 23% of the world's total energy consumption originates from tribological contacts. Of that, 20% is used to overcome friction, and 3% is used to remanufacture worn parts and spare equipment due to wear and wear-related failures [8]. Nonetheless, according to Holmberg [4], 28% of the fuel energy is wasted

in an average passenger car due to direct contact (with braking friction excluded). The internal combustion engine alone is responsible for around one-third (30 to 35%) of the total friction losses in a passenger car. From this, most of the friction losses (45%) are consumed in the piston assembly. Therefore, an obvious way to reduce fuel consumption is the reduction of friction losses in the piston ring–cylinder liner assembly. For this reason, choosing appropriate tribopairs for the piston ring–cylinder liner contact is an excellent way to optimize the tribosystem [9].

Conventional coating material for the piston ring part mainly uses chromium-based coatings and, more recently, DLC coatings [10]. The DLC coating represents one of the most advantageous carbon-based material solutions. Its amorphous structure combines graphite (providing superlubricity) and diamond (offering a high hardness), which are both required for good wear resistance [11]. Compared with the conventional CrN coatings, its superior tribological resistance increases the service life and improves the piston ring's performance [12]. Due to those excellent tribological properties, the DLC coating solution was adopted as a protective material for piston rings as an alternative to chromium-based solutions [11]. Although the DLC coatings deposited over the surface of the piston rings are often produced by arc deposition [13], in this work, the optimized DLC coating used was produced by sputtering. Arc deposition allows a higher sp2/sp3 ratio, boosting their hardness to the maximum. Indeed, a higher and lower sp2/sp3 ratio is related to a more lubricious behavior or a harder and more resistant surface [14]. However, arc deposition is well known to produce droplets, which are often reported to lead to the coatings' early/premature failure [11,15]. Sputtering deposition was thus used (i) to avoid the problems often caused by the presence of droplets; (ii) because it allows a lower sp2/sp3 ratio, which improves friction, although it decreases hardness; and (iii) because it is a well-established and widespread technology to coat a wide range of components for different applications, and therefore, it is of industrial interest to test solutions produced with the same sputtering deposition setup. It should be noted that the cost of the thin solid coating solution technology is extremely high, and enterprises choose to acquire the most versatile technology.

Over the last decades, tribologists have developed and investigated new low-friction coatings due to the eminent need for friction and wear reduction and greener and more innovative industrial solutions [16–18]. Those efforts rendered fruitful results in the form of the most famous low-friction coatings. i.e., transition metal dichalcogenides (TMDs) [19–26]. TMDs are solid lubricant materials, specifically intrinsic solid lubricants, whose crystal structure facilitates interfacial sliding/shear to achieve low friction and wear in sliding contacts and low torque in rolling contacts [27]. They are known as excellent dry lubricants, forming a thin tribolayer that simultaneously protects the coating [28]. The TMDs have a weak bond (Van der Waals) force within the structure. This unique bonding characteristic leads to easy slipping of different layers, resulting in low friction. TMDs are not used/recommended in pure form due to their low load-bearing capabilities, low hardness, and susceptibility to environmental degradation during sliding in diverse environments [29]. Thus, after extensive efforts, researchers introduced C- and N-doped TMD coatings as possible solutions for the abovementioned problems. These efforts rendered excellent results; therefore, optimized C- and N-alloyed TMD coatings have been reported in the past few years [30–32]. Although extensive research has been carried out on those coatings, a study comparing the tribological performance of TMDs and DLC is still missing from the literature. At the same time, there is limited research on the potential application of TMDs in the piston rings of internal combustion engines.

The current research investigates the tribological performance of various TMD coatings doped with carbon (WSC and MoSeC) and nitrogen (WSN and MoSeN), comparing them to a conventional DLC (diamond-like carbon) coating. The tribological tests were performed under dry and lubricated conditions, and the results regarding friction and wear properties were examined. One of the main objectives is to provide a starting point for the discussion of using TMD coating instead of DLC for piston ring–cylinder liner contact in internal

combustion engines. In this study, minimizing friction is crucial for efficiency, leading to reduced fuel consumption, while maximizing wear resistance is essential for durability, ensuring a longer service life for the piston ring.

2. Materials and Methods

2.1. Coating Deposition Parameters and Properties

Coatings based on C- and N-doped TMD (WSC, WSN, MoSeC, and MoSeN) and DLC were deposited by PVD sputtering (TEER Coating). The coatings were produced at IPN—Instituto Pedro Nunes, Portugal, a non-profit institution that interfaces with the industry and has a wide range of optimized coating solutions for different applications. The chamber used for the depositions had four cathodes evenly distributed in relation to the chamber's center, performing unbalanced close-field magnetron sputtering using DC power supplies. The purity of all targets used in the depositions was approximately 99.99%, and the coatings were deposited on polished M2 steel discs with a diameter of 25 mm and a thickness of 8 mm. Before the depositions, these substrates underwent an ultrasonic cleaning process involving 15 min of acetone and ethanol bath exposure. The specimens were then mounted on the rotating substrate holder of the chamber and revolved at 10 rpm in its shaft. The distance from the substrates to the targets was kept at 150 mm for all the depositions. The chamber was then evacuated down to a base pressure lower than 0.003 Pa. The substrates were then etched with Ar ions for 40 min, applying −600 V to the substrate table at a frequency of 250 kHz and a reverse time of 1.6 µs with a pulsed DC power supply (Pinnacle Plus, Advanced Energy) to remove contamination. Simultaneously, the different targets used for the depositions were cleaned by applying power to each of them while having the shutters in front to avoid substrate contamination. For each coating, before the final layer deposition, an interlayer and a gradient layer with chromium were deposited to improve the coating's adhesion to the substrate. After that, the final coating layers were deposited. Wavelength dispersive spectroscopy (WDS) was used to determine the elemental composition of the coatings. The WDS detector was coupled to a field emission scanning electron microscope (FESEM) and operated using INCA software (https://www.etas.com/). The analysis was conducted with an accelerating voltage of 15 kV. Table 1 presents the main deposition parameters, hardness, and elemental compositions of the analyzed coatings. It also includes references where additional information on optimizing these coatings can be found.

Table 1. Coating designations, main deposition parameters, properties, and references.

Coating	Base Pressure (Pa)	Working Pressure (Pa)	Elemental Composition (%)			Hardness (GPa)	Thickness (µm)	Reference (DOI)
DLC	0.0003	0.37 (Ar)	C: 99.3	O: 0.7		21.4	2	10.1016/j.diamond.2016.10.024
MoSeN	0.0004	0.26 (Ar + N)	Mo: 26	Se: 41	N: 33	4.8	2	10.1016/j.matlet.2022.131967
MoSeC	0.0003	0.31 (Ar)	Mo: 52	Se: 30	C: 18	7.2	1.8	10.1016/j.surfcoat.2020.125889
WSN	0.0003	0.27 (Ar + N)	W: 39	S: 38	N: 23	4.6	1	10.1016/j.jmrt.2022.02.116
WSC	0.0003	0.3 (Ar)	W: 19	S: 31	C: 50	5.8	1.8	10.1016/j.triboint.2020.106363

The roughness (arithmetic [Ra] and root mean square roughness [Rq]) of the samples surfaces used in the block-on-ring (BoR) tests was measured using a surface measuring instrument (Mitutoyo—Surftest SJ-500), as shown in Table 2. The directions of the measurements were the same as the relative motion during the BoR tests.

Table 2. Coating designations, main deposition parameters, and properties.

Coating	Ra [μm]	Rq [μm]
DLC	0.032 ± 0.002	0.042 ± 0.003
WSC	0.028 ± 0.002	0.036 ± 0.002
WSN	0.034 ± 0.001	0.044 ± 0.001
MoSeC	0.026 ± 0.002	0.035 ± 0.002
MoSeN	0.021 ± 0.003	0.026 ± 0.003
Ring	0.261 ± 0.026	0.323 ± 0.035

2.2. Coatings' Tribological Performance

Two test conditions, dry and lubricated, were designed for the tribological tests. A load scanner (LS) test was used in dry conditions; the objective was to evaluate the wear mechanism in the absence of lubricant. This condition was set to reproduce a "lubrication failure", thereby generating scuffing, which is characterized by localized damage caused by solid phase welding between sliding surfaces without local surface fusion [33]. Scuffing can also occur due to very high temperatures, causing a reduction in lubricant viscosity and material properties [34,35].

To test the coatings in a lubricated condition, a block-on-ring (BoR) tester was used under low sliding velocity (0.05 m/s) to reproduce mixed and boundary lubrication conditions, similar to what occurs near a piston's dead points. In this way, the aim was to subject the coatings to more severe conditions, i.e., higher friction and wear.

In the LS tests (Figure 1a), a steel ball (AISI 52100) with a diameter of 5.5 mm and a roughness of Ra = 0.025 μm (ANSI/AFBMA 10-1983, grade 10) was slid against the coatings for a stroke length of 8 mm (sliding velocity of 0.44 mm/s). A progressively increasing normal force ranging from 0 to 45 N was used. The normal and friction forces were measured and allowed the calculation of the friction coefficient throughout the sliding process. The wear marks produced on the coatings and balls were analyzed using a 3D digital microscope (Hirox, HRX-01) and a scanning electron microscope (Hitachi, SU3800) equipped with energy-dispersive spectroscopy (Bruker, Quantax).

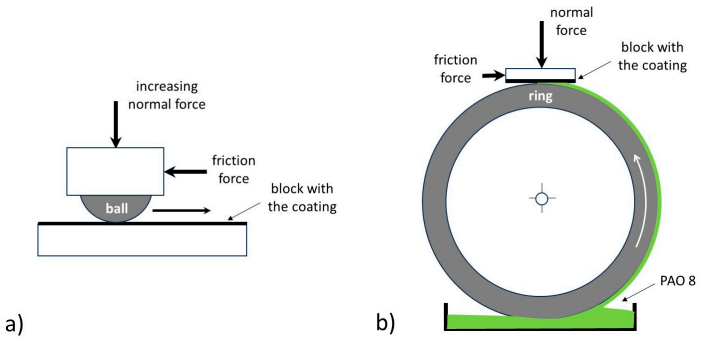

Figure 1. Representative schemes/illustrations of the (**a**) load scanner (LS) and (**b**) block-on-ring (BoR) tests.

For the lubricated tests performed on the BoR (Figure 1b), a ring made of AISI 3415 annealed steel, with hardness 244 ± 2.8 HV2 (Duramin, Struers), was used. This ring had an outer diameter of 115 mm and was 12 mm wide. The ring rotated to produce a relative velocity of 0.05 m/s against the coated blocks, low enough to minimize hydrodynamic effects [36]. A synthetic oil (polyalphaolefin—PAO 8) without additives was used as a lubricant so that it could interfere with the contact mechanisms between the ring and the coatings. The temperature of the ring was controlled at three different levels during the BoR tests: 20 °C, 60 °C, and 100 °C. The increase in the temperature of the ring—and consequently of the oil in contact with the block—was intended to reduce the oil's viscosity,

thereby inducing wear processes and increasing friction. The BoR tests were performed under a normal force of 10 N between the block and the ring, resulting in an average contact stress of 19 MPa, according to the Hertz theory of contact for purely normal loading of solids [37–39]. The total sliding distance of each run was 196 m. Data were recorded using a data acquisition device (National Instruments, USB 6009) with an acquisition sampling rate set at 1 kHz. A total of 7200 points per revolution were used for post-processing analysis. A summary of the operational parameters used in the BoR tests is shown in Table 3.

Table 3. Summary of the operating parameters used in the block-on-ring (BoR) tests.

Temperature [°C]	Repetitions [-]	Normal Force [N]	Sliding Velocity [m/s]	Total Sliding Distance [m]
20	6	10	0.05	196
60	3			
100	3			

A novel procedure was created for the wear analysis of the coatings in the post-BoR tests. It comprises three steps (Figure 2): In Step 1, images of the wear scars on the block surface were captured using a 3D digital optical microscope (Hirox, HRX-01). In Step 2, a micrograph of each block was subjected to the image segmentation technique, making it possible to highlight each wear scar separately. A Python script (named "code 1") was used for this purpose. This script is based on Otsu's algorithm, and it was previously used and validated in previous studies [40,41]. Step 3, the binarized image of each block was processed through a second script, also coded in Python and named "code 2". This code calculates the wear volume of each scar based on the volume of the circular segment of the ring that penetrates the block. Still regarding step 3, the Python script (code 2) was based on the measurement of the scar width (ω) as a function of the length (x) of the wear scar. Equations (1) and (2) exhibit the mathematical expressions implemented in the Python script (code 2).

$$V = \sum_{i=1}^{N} \left(\frac{R^2}{2} (\theta_i - \sin \theta_i) \right) \Delta x \quad (1)$$

$$\theta_i = 2 \sin^{-1} \left(\frac{\omega_i}{2R} \right) \quad (2)$$

where V is the wear volume [μm3], N is the total number of segments (pixels) that comprise the scar length [-], R is the radius of the ring [μm], θ_i is the angle of the wear scar in each segment [rad], ω_i is the scar width in each segment [μm] and Δx is the distance between segments (pixel resolution) [μm].

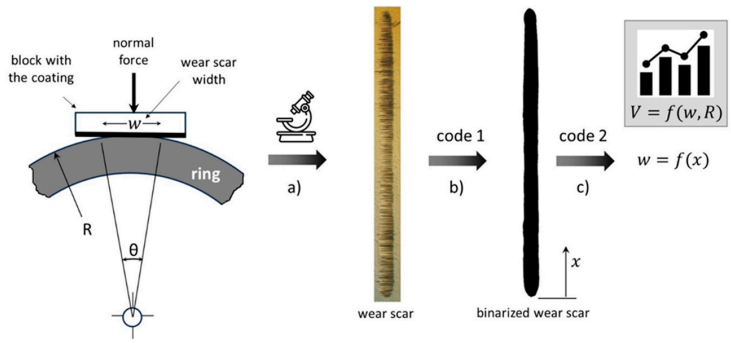

Figure 2. Illustration of the methodology used to estimate the average volume loss V (in mm^3) in the wear scars: (**a**) each wear scar is captured under an optical microscope; (**b**) the image is binarized to a black and white image using code 1; (**c**) code 2 determines the width of the wear scar along the length of the wear mark and calculates the volume (this figure shows a wear mark in MoSeN, tested at 20 °C).

3. Results

3.1. Load Scanner (LS) Results

The dry friction results obtained in the LS tests are shown in Figure 3. At the beginning of the LS test (from 0 to 2 mm), friction displayed high oscillations due to the running-in effect, i.e., the adaptation of the surfaces of the coating and the ball by breakage of asperities until the steady-state stage was reached. After 2 mm of displacement, with normal forces greater than 11.25 N, friction became more stable (average values shown in Figure 3b). However, in the stable phase (after 2 mm), DLC presented more oscillations than TMDs. In this dry test, the friction of the TMDs coatings was quite similar, with an average of 0.095, which is around 30% of that observed for the DLC coating (0.33). In wear tests where the counterbody repeatedly passes over the coating, the low friction of in TMD coatings is mainly attributed to the formation of a low-shear-strength interface (tribolayer) over the surfaces in contact [27,42]. However, in the case of the LS test, only a single pass of the ball on the coatings occurred. Therefore, the low friction observed for the TMD coatings in the LS tests was due to their shearable planes, which align near the surface and are recognized as an intrinsic characteristic of this type of coating.

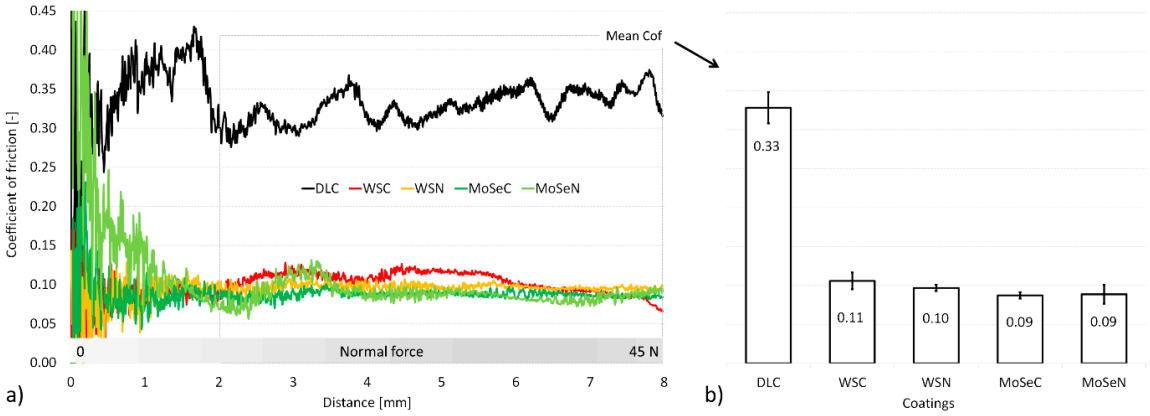

Figure 3. Friction coefficient measured in the LS tests for all coatings. (**a**) Friction coefficient as a function of sliding distance and applied normal force; (**b**) average value between 2 and 8 mm (normal load: 11 to 45 N; average contact pressure: 1.02 to 1.65 GPa).

The friction and wear marks of the DLC coating in the LS test are correlated and explored in more detail in Figure 4. As the worn tracks of the TMDs were imperceptible in the LS tests, this type of analysis was not possible to conduct for those coatings.

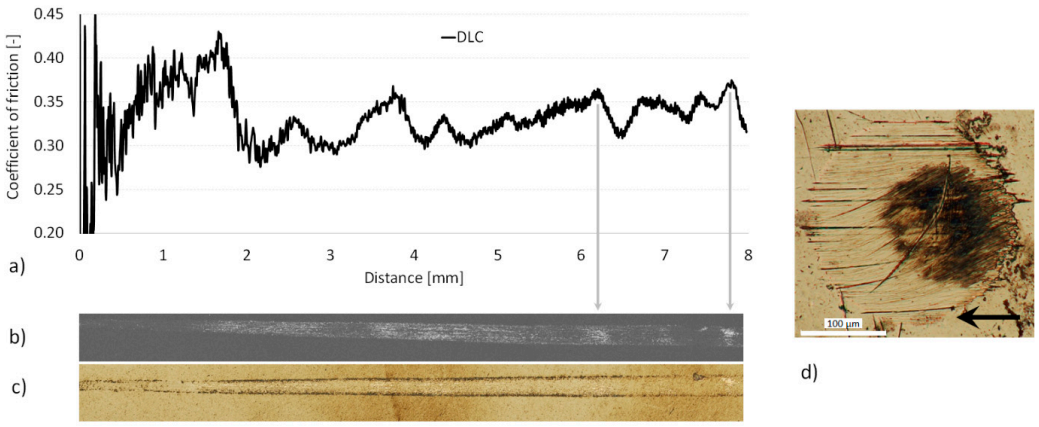

Figure 4. Detail of friction coefficient and wear obtained for the DLC coating in the LS test. (**a**) Coefficient of friction as a function of distance; (**b**) worn track seen via scanning electron microscopy (SEM); (**c**) worn track seen via digital optical microscopy; (**d**) wear scar on the steel ball.

As shown in Figure 4, the LS test produced a significant mark on the DLC coating. When observing the path using scanning electron microscopy (Figure 4b), patterns suggested the adhesion of the steel ball material over the worn track. At the beginning of the displacement, friction was relatively high and unstable. After this running-in period (around 2 mm), the adhesion process began, with an increase in the magnitude of the friction force induced by the growth of the agglomerated material in front of the ball. When the material accumulated in front of the sphere reached a critical dimension and finds anchoring points, dunes of adhering material were formed, with a reduction in the friction force. Fluctuations in friction occurred from a distance of 2 to 8 mm. They were characterized by some rapid increase in friction, whose moment coincided with a greater amount of material adhering to the track, as seen in the places marked by gray arrows. The worn mark on the sphere had a circular shape with a diameter of 240 µm (Figure 4d).

Figure 5 shows a detailed analysis (including elemental analysis) of the wear track of the DLC coating. As shown in the EDS of Figure 5d, the material adhered to the DLC coating indicated the presence of iron, which suggested the material attached to the steel ball counterpart. The absence of chromium (Figure 5c) from the intermediate DLC layer indicated that the material substrate (M2 steel) was not reached, confirming that the iron originated from the ball. Since DLC showed adhesion in the absence of lubrication, it may indicate a propensity for scuffing when applied to cylinder rings. TMD coatings, on the other hand, did not show this propensity, since they did not show any wear marks in this dry test.

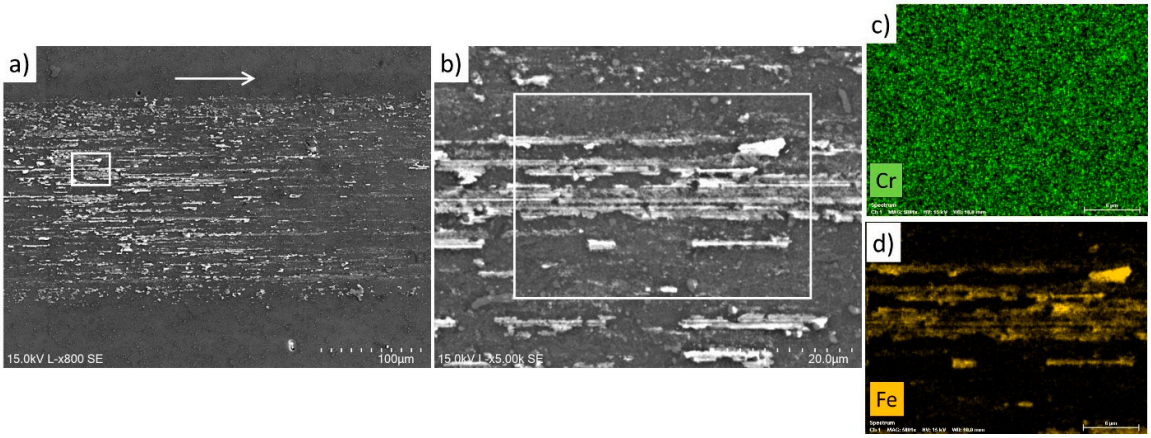

Figure 5. Wear analysis of DLC coating. (**a**) Scanning electron microscopy; (**b**) detail emphasizing adhered material; (**c**) chromium map derived from energy-dispersive spectroscopy (EDS); (**d**) iron map derived from EDS.

3.2. Block-on-Ring (BoR) Results

The performance of the coatings under lubricated conditions was evaluated using the block-on-ring (BoR) tester. Figure 6a illustrates the friction coefficients measured in the BoR tests using oil at different temperatures. In this graph, the error bar represents the standard deviation of the CoF considering all runs performed as each temperature (six repetitions at 20 °C and three repetitions at 60 and 100 °C). An increase in friction was noticeable at 60 °C compared to 20 °C and 100 °C for C-doped TMD coatings, specifically MoSeC and WSC. The rise in oil temperature from 20 to 60 °C reduced the oil's viscosity, subjecting the contact surfaces to more direct contact between asperities during the boundary lubrication regime. However, another phenomenon appeared to prevail at a temperature of 100 °C, since the friction reduced to the same level as 20 °C. A possible explanation is the formation of a film adsorbed on the surface at the highest temperature (100 °C), which may be the product of a chemical reaction with carbon. This hypothesis will be the subject of further investigation. This friction rise at 60 °C was not observed in N-doped TMD coatings. When considering the average of the friction values measured in the twelve tests (temperatures from 20 to 100 °C—Figure 6b), the DLC coating produced greater friction than most TMD

coatings, a behavior already verified in the dry tests (Figure 3b). The WSN coating also presented greater friction, resembling that of the DLC coating.

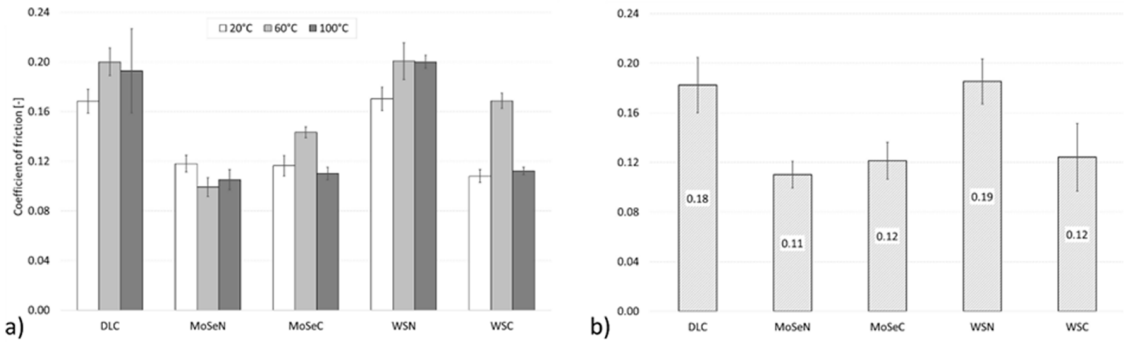

Figure 6. Coefficients of friction obtained in the BoR tests. (**a**) Coefficients of friction at 20, 60, and 100 °C; (**b**) mean CoF, considering all three temperatures.

The friction analysis provides insight into the efficiency performance of the studied coatings. However, the durability of these materials is crucial for a comprehensive comparative analysis, especially for their application in piston rings. Therefore, the wear of the coatings measured in the BoR tests was also accessed.

Figure 7 shows the wear rate of the coatings obtained in the BoR tests for the different temperatures tested. DLC showed the best wear resistance among all coatings in the BoR tests. It is worth noting that DLC is well known for its exceptional wear properties, primarily attributed to its high surface hardness and robust bond with the interlayer. In this study, the surface hardness of DLC was observed to be 3.8 times higher than that of TMDs, potentially accounting for the superior wear performance of DLC in the BoR tests.

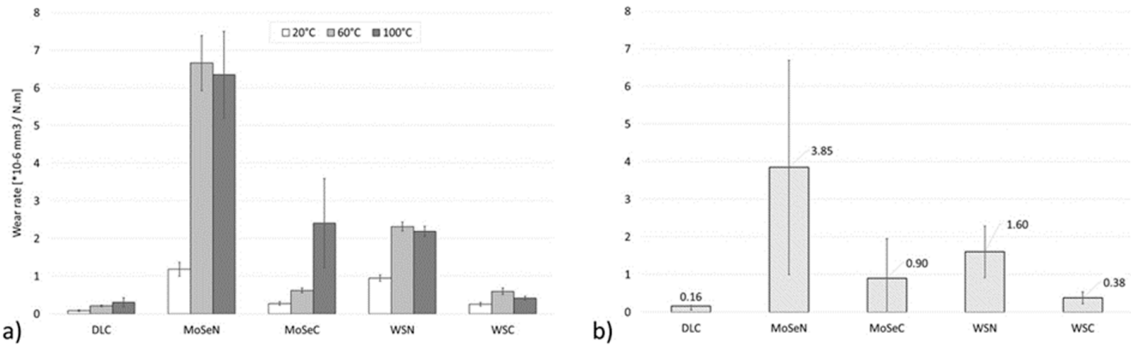

Figure 7. Wear rate results measured in the BoR tests. (**a**) Wear rates at 20, 60, and 100 °C, (**b**) mean wear rate.

On the other hand, the negative highlight in terms of wear in the BoR tests was the performance of MoSeN. Although this coating showed lower friction coefficients (Figure 6), MoSeN presented a higher wear rate, especially at 60 and 100 °C. These high wear rates (above 60 °C) resulted in the rupture of the 2.2 µm thin-film layer in the respective tests (totaling six runs), as verified by SEM/EDS (Figure 8). Chemical analysis of the deepest regions of the worn track (Figure 8c) detected iron from the substrate (M2 steel), as well as chromium from the interlayer used to increase the adhesion of the coating to the substrate. The main elements of the coating (Mo and Se) appear naturally in the worn regions (Figure 8b).

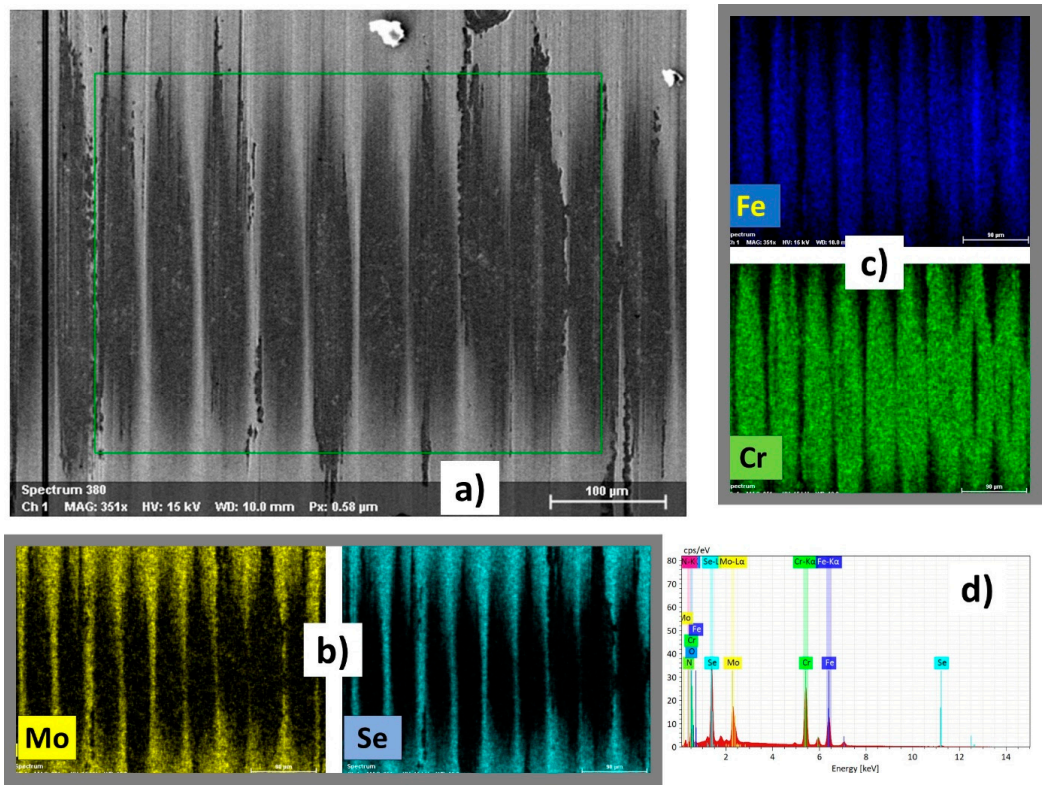

Figure 8. Wear analysis showing the rupture of the MoSeN coating (test condition: 100 °C). (**a**) Image acquired using scanning electron microscopy (SEM), showing the region analyzed by energy dispersive spectroscopy (EDS). (**b**) Main elements of the coating (Mo and Se) identified by EDS. (**c**) Substrate and interlayer elements (Fe and Cr) identified by EDS. (**d**) Spectrum of elements identified by EDS.

The coating with the second-highest wear was WSN, and no instances were detected in which the coating wore out. However, the same cannot be said for the MoSeC coating, as a 1.8 µm coating wore out at 100 °C, as depicted in Figure 9. For the other coatings, no wear points were seen exceeding the coatings' thickness. It is worth noting that the DLC and WSC coatings exhibited the lowest wear rates, as illustrated in Figure 7b.

For a complete tribological analysis, the friction and wear performance of each coating obtained in the BoR tests were correlated, as shown in Figure 10. As mentioned previously, the MoSeN film layer suffered localized wear that exceeded the thickness of the coating layer in all six tests performed at temperatures above 60 °C, while MoSeC exhibited such rupture in only one case, performed at 100 °C. These premature failures occurred at wear rates greater than 3×10^{-6} mm^3/Nm, as indicated by a dashed line in Figure 10a. Considering a worn-out coating as a disqualifying criterion, the coatings that remain under discussion in the application under study are the WS-based TMD (WSC and WSN) coatings and the DLC (reference coating). However, the WSN presented relatively high wear and friction, making it a less qualified option. Therefore, the coatings with the best tribological performance were WSC and DLC. Based on Figure 10, it can be seen that the wear rate of WSC was 130% higher than that of the DLC. However, the lubricated friction was 30% lower than that of the DLC coating (WSC = 0.124; DLC = 0.18). This reduction in friction combined with the absence of material adhering to the film from the counterpart is an indication of a reduction in the risk of scuffing, making it a promising solution for replacing the DLC coating to protect the surface of the cylinder piston rings, used in combustion engines.

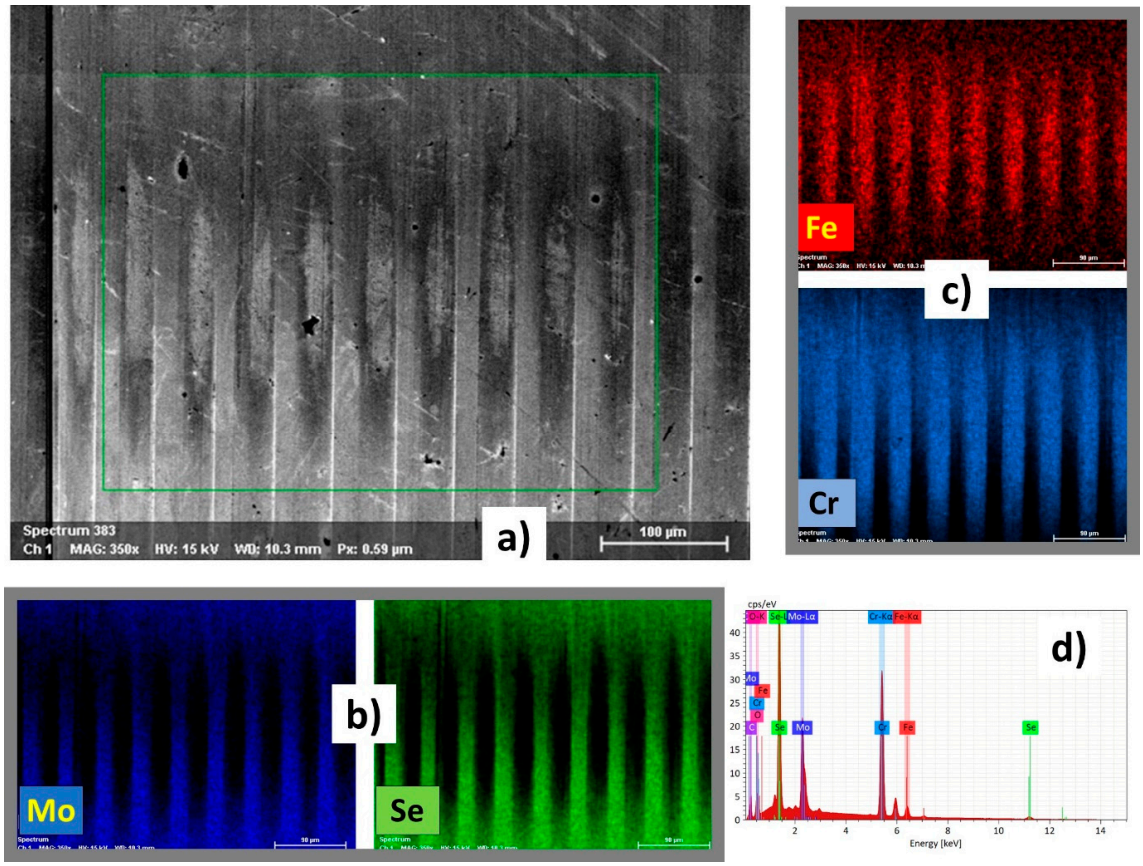

Figure 9. Wear analysis showing the rupture of the MoSeC coating (test condition: 100 °C). (**a**) Image acquired using scanning electron microscopy (SEM), showing the region analyzed by energy dispersive spectroscopy (EDS). (**b**) Main elements of the coating (Mo and Se) identified by EDS. (**c**) Substrate and interlayer elements (Fe and Cr) identified by EDS. (**d**) Spectrum of elements identified by EDS.

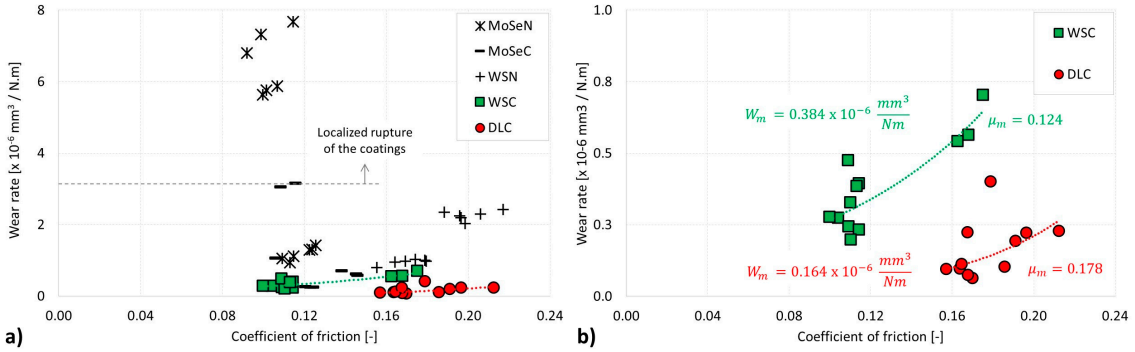

Figure 10. Wear and coefficient of friction obtained in the BoR test: (**a**) all coatings; (**b**) DLC and WSC.

4. Conclusions

Load scanner tests (LS tests) demonstrated that the DLC coating is susceptible to adhesive wear of the metal counterpart in the absence of lubrication. This condition is similar to that in the contact between the engine ring and cylinder when there is a lubrication failure, resulting in the catastrophic failure known as scuffing. Under the same testing conditions, adhesion was not observed for TMD coatings. Therefore, we can conclude that the DLC coating is susceptible to scuffing, a disadvantage not presented by the TMD coatings selected in this study.

In the BoR tests performed under low speed in lubricated conditions, DLC exhibited the best wear resistance. This was mainly attributed to its higher hardness magnitude,

which is 3.8 times higher than that of the TMDs selected in the present investigation. On the other hand, WSC, MoSeC, and MoSeN exhibited lower friction than DLC under lubricated conditions (BoR tests), whereas under dry sliding conditions (LS tests), all studied TMDs (including WSN) presented lower friction than the DLC coating. MoSe-based TMD coatings exhibited the poorest wear performance in the BoR tests, including localized wear beyond the coating layer.

Among the studied TMD coatings, WSC was the only one that showed wear performance comparable to that of the reference coating (DLC). Despite the wear rate of WSC being 130% higher than that of DLC, it exhibited lubricated friction approximately 30% lower than that of the DLC coating (WSC = 0.124; DLC = 0.18). This reduction in friction may lead to decreased fuel consumption in combustion engines. Additionally, the low or non-existent risk of cylinder metal adhesion to the WSC coating is favorable for this coating, as it reduces the risk of adhesive wear (i.e., scuffing). Therefore, among the various TMD coating options, WSC is a promising candidate for replacing DLC in cylinder rings.

Author Contributions: N.F.F.—Conceptualization, Methodology, Investigation, Formal Analysis, Writing—Original Draft, Writing—Review and Editing. P.D.N.—Writing—Original Draft, Writing—Review and Editing. J.C.P.—Investigation, Writing—Review and Editing. F.F.—Conceptualization, Resources, Writing—Review and Editing. T.B.Y.—Methodology, Investigation. A.C.—Resources. L.V.—Writing—Review and Editing. A.R.—Supervision, Conceptualization, Resources, Writing—Review and Editing. All authors have read and agreed to the published version of the manuscript.

Funding: CEMMPRE—ref. "UIDB/00285/2020" and LA/P/0112/2020 projects, sponsored by FEDER funds through the COMPETE program—Operational Program on Competitiveness Factors and by national funds through FCT—Foundation for Science and Technology, are acknowledged. This study was financed in part by the Coordenação de Aperfeiçoamento de Pessoal de Nível Superior—Brasil (CAPES)—Finance Code 001 and by the Conselho Nacional de Desenvolvimento Científico e Tecnológico—Brasil (CNPq).

Institutional Review Board Statement: Not applicable.

Informed Consent Statement: Not applicable.

Data Availability Statement: The data presented in this study are available on request from the corresponding author. The data are not publicly available due to privacy.

Conflicts of Interest: The authors declare that they have no known competing financial interests or personal relationships that could have appeared to influence the work reported in this paper.

References

1. Jost, H.P. Tribology—Origin and Future. *Wear* **1990**, *136*, 1–17. [CrossRef]
2. Duncan, D. *History of Tribology*; Wiley: Hoboken, NJ, USA, 1998; ISBN 978-1-86058-070-3.
3. Echávarri, J.; De La Guerra, E.; Chacón, E. Tribology: A Historical Overview of the Relation between Theory and Application. In *A Bridge between Conceptual Frameworks*; Pisano, R., Ed.; History of Mechanism and Machine Science; Springer: Dordrecht, The Netherlands, 2015; Volume 27, pp. 135–154. ISBN 978-94-017-9644-6.
4. Holmberg, K.; Andersson, P.; Erdemir, A. Global Energy Consumption Due to Friction in Passenger Cars. *Tribol. Int.* **2012**, *47*, 221–234. [CrossRef]
5. Holmberg, K.; Andersson, P.; Nylund, N.-O.; Mäkelä, K.; Erdemir, A. Global Energy Consumption Due to Friction in Trucks and Buses. *Tribol. Int.* **2014**, *78*, 94–114. [CrossRef]
6. Holmberg, K.; Siilasto, R.; Laitinen, T.; Andersson, P.; Jäsberg, A. Global Energy Consumption Due to Friction in Paper Machines. *Tribol. Int.* **2013**, *62*, 58–77. [CrossRef]
7. Holmberg, K.; Kivikytö-Reponen, P.; Härkisaari, P.; Valtonen, K.; Erdemir, A. Global Energy Consumption Due to Friction and Wear in the Mining Industry. *Tribol. Int.* **2017**, *115*, 116–139. [CrossRef]
8. Holmberg, K.; Erdemir, A. Influence of Tribology on Global Energy Consumption, Costs and Emissions. *Friction* **2017**, *5*, 263–284. [CrossRef]
9. Ferreira, A.R.M. New Processing Technologies for Improved Compression Piston Ring Performance. Doctoral Dissertation, University of Minho, Guimarães, Portugal, 2021.
10. Ferreira, R.; Martins, J.; Carvalho, Ó.; Sobral, L.; Carvalho, S.; Silva, F. Tribological Solutions for Engine Piston Ring Surfaces: An Overview on the Materials and Manufacturing. *Mater. Manuf. Process.* **2020**, *35*, 498–520. [CrossRef]

11. Ferreira, R.; Almeida, R.; Carvalho, Ó.; Sobral, L.; Carvalho, S.; Silva, F. Influence of a DLC Coating Topography in the Piston Ring/Cylinder Liner Tribological Performance. *J. Manuf. Process.* **2021**, *66*, 483–493. [CrossRef]
12. Tung, S.C.; Gao, H. Tribological Characteristics and Surface Interaction between Piston Ring Coatings and a Blend of Energy-Conserving Oils and Ethanol Fuels. *Wear* **2003**, *255*, 1276–1285. [CrossRef]
13. Bruno, R.A.; Rabello, R.B.; Silva, D.A.; Araujo, J.A. DLC Coated Ring Pack for Heavy Duty Diesel Engines. In *Blucher Engineering Proceedings*; Editora Blucher: São Paulo, Brasil, 2017; pp. 462–476.
14. Rao, X.; Yang, J.; Chen, Z.; Yuan, Y.; Chen, Q.; Feng, X.; Qin, L.; Zhang, Y. Tuning C–C Sp2/Sp3 Ratio of DLC Films in FCVA System for Biomedical Application. *Bioact. Mater.* **2020**, *5*, 192–200. [CrossRef]
15. Takikawa, H.; Izumi, K.; Miyano, R.; Sakakibara, T. DLC Thin Film Preparation by Cathodic Arc Deposition with a Super Droplet-Free System. *Surf. Coat. Technol.* **2003**, *163–164*, 368–373. [CrossRef]
16. Heshmat, H.; Hryniewicz, P.; Walton Ii, J.F.; Willis, J.P.; Jahanmir, S.; DellaCorte, C. Low-Friction Wear-Resistant Coatings for High-Temperature Foil Bearings. *Tribol. Int.* **2005**, *38*, 1059–1075. [CrossRef]
17. Zhang, Y.; Hou, W.; Yu, J.; Chen, C.; Zhou, L. The Role of Carbon in Wear Resistance of $CoCrFeNiTi_{0.5}$ High-Entropy Alloy Layer. *J. Mater. Eng. Perform.* **2024**. [CrossRef]
18. Zhen-yu, Z.; Zhi-guo, J.; Qiu-yang, Z.; Yu, L.; Zhi-peng, Y.; Cong, D.; Zhong-yu, P. Research on the Construction of Gradient Nanostructure and Anti-Tribocorrosion Behavior of Aluminum Alloy Surface. *Tribol. Int.* **2024**, *194*, 109448. [CrossRef]
19. Gustavsson, F.; Jacobson, S. Diverse Mechanisms of Friction Induced Self-Organisation into a Low-Friction Material—An Overview of WS_2 Tribofilm Formation. *Tribol. Int.* **2016**, *101*, 340–347. [CrossRef]
20. Scharf, T.W. Transition Metal Dichalcogenide-Based (MoS_2, WS_2) Coatings. In *ASM Handbook—Friction, Lubrication, and Wear Technology*; Totten, G.E., Ed.; ASM International: Almere, The Netherlands, 2017; Volume 18, p. 14.
21. Vaziriserehk, M.R.; Martini, A.; Strubbe, D.A.; Baykara, M.Z. Solid Lubrication with MoS_2: A Review. *Lubricants* **2019**, *7*, 57. [CrossRef]
22. Hudec, T. Transition Metal Dichalcogenide-Based Solid Lubricant Coatings Prepared by High Target Utilisation Sputtering. Doctoral Dissertation, University of Southampton, Southampton, UK, 2021.
23. Fominski, V.; Fominski, D.; Demin, M.; Romanov, R.; Goikhman, A. Enhanced Tribological Performance of Low-Friction Nanocomposite WSexSy/NP-W Coatings Prepared by Reactive PLD. *Nanomaterials* **2023**, *13*, 1122. [CrossRef]
24. Wang, R.; Zhang, F.; Yang, K.; Xiong, Y.; Tang, J.; Chen, H.; Duan, M.; Li, Z.; Zhang, H.; Xiong, B. Review of Two-Dimensional Nanomaterials in Tribology: Recent Developments, Challenges and Prospects. *Adv. Colloid Interface Sci.* **2023**, *321*, 103004. [CrossRef]
25. Li, M.; Zhou, Q.; Cao, M.; Zhou, Z.; Liu, X. High-Temperature Solid Lubrication Applications of Transition Metal Dichalcogenides(TMDCs) MX_2: A Review. *Nano Mater. Sci.* **2024**. [CrossRef]
26. Mukhtar, S.H.; Gulzar, A.; Saleem, S.; Wani, M.F.; Sehgal, R.; Yakovenko, A.A.; Goryacheva, I.G.; Sharma, M.D. Advances in Development of Solid Lubricating MoS_2 Coatings for Space Applications: A Review of Modeling and Experimental Approaches. *Tribol. Int.* **2024**, *192*, 109194. [CrossRef]
27. Scharf, T.W.; Prasad, S.V. Solid Lubricants: A Review. *J. Mater. Sci.* **2013**, *48*, 511–531. [CrossRef]
28. Yaqub, T.B. Optimization of Sputtered Mo-Se-C Coatings for Efficient Self-Adaptation during Sliding in Diverse Enviroments. Doctoral Dissertation, Universidade de Coimbra, Coimbra, Portugal, 2020.
29. Polcar, T.; Cavaleiro, A. Review on Self-Lubricant Transition Metal Dichalcogenide Nanocomposite Coatings Alloyed with Carbon. *Surf. Coat. Technol.* **2011**, *206*, 686–695. [CrossRef]
30. Hebbar Kannur, K.; Yaqub, T.B.; Pupier, C.; Héau, C.; Cavaleiro, A. Mechanical Properties and Vacuum Tribological Performance of Mo–S–N Sputtered Coatings. *ACS Appl. Mater. Interfaces* **2020**, *12*, 43299–43310. [CrossRef]
31. Araujo, J.A.; Araujo, G.M.; Souza, R.M.; Tschiptschin, A.P. Effect of Periodicity on Hardness and Scratch Resistance of CrN/NbN Nanoscale Multilayer Coating Deposited by Cathodic Arc Technique. *Wear* **2015**, *330–331*, 469–477. [CrossRef]
32. Lin, J.; Wei, R.; Bitsis, D.C.; Lee, P.M. Development and Evaluation of Low Friction TiSiCN Nanocomposite Coatings for Piston Ring Applications. *Surf. Coat. Technol.* **2016**, *298*, 121–131. [CrossRef]
33. Ludema, K.C. A Review of Scuffing and Running-in of Lubricated Surfaces, with Asperities and Oxides in Perspective. *Wear* **1984**, *100*, 315–331. [CrossRef]
34. Shuster, M.M.; Stong, T.; Deis, M.C.; Burke, D.C. *Piston Ring Cylinder Liner Scuffing Phenomenon: Investigation, Simulation and Prevention*; SAE International: Warrendale, PA, USA, 1 March 1999; No. 1999-01-1219.
35. Zhang, W.; Becker, E.; Wang, Y.; Zou, Q.; Zhou, B.; Barber, G.C. Investigation of Scuffing Resistance of Piston Rings Run against Piston Ring Grooves. *Tribol. Trans.* **2008**, *51*, 621–626. [CrossRef]
36. Adachi, K.; Hutchings, I.M. Sensitivity of Wear Rates in the Micro-Scale Abrasion Test to Test Conditions and Material Hardness. *Wear* **2005**, *258*, 318–321. [CrossRef]
37. Hertz, H. Über Die Berürung Fester Elastischer Körper. *J. Für Die Reine Und Angew. Math.* **1881**, *92*, 156–171.
38. Horowitz, A. A Contribution to the Engineering Design of Machine Elements Involving Contrashaped Contacts. *Isr. J. Technol.* **1971**, *9*, 311–322.
39. Savkoor, A.R. Models of Friction. In *Handbook of Materials Behavior Models*; Elsevier: Amsterdam, The Netherlands, 2001; pp. 700–759, ISBN 978-0-12-443341-0.

40. Neis, P.D.; Ferreira, N.F.; Fekete, G.; Matozo, L.T.; Masotti, D. Towards a Better Understanding of the Structures Existing on the Surface of Brake Pads. *Tribol. Int.* **2017**, *105*, 135–147. [CrossRef]
41. Poletto, J.C.; Barros, L.Y.; Neis, P.D.; Ferreira, N.F. Analysis of the Error in the Estimation of the Morphology of Contact Plateaus Existing on the Surface of Brake Pads. *Tribol. Int.* **2018**, *126*, 297–306. [CrossRef]
42. Yaqub, T.B.; Vuchkov, T.; Bruyère, S.; Pierson, J.-F.; Cavaleiro, A. A Revised Interpretation of the Mechanisms Governing Low Friction Tribolayer Formation in Alloyed-TMD Self-Lubricating Coatings. *Appl. Surf. Sci.* **2022**, *571*, 151302. [CrossRef]

Disclaimer/Publisher's Note: The statements, opinions and data contained in all publications are solely those of the individual author(s) and contributor(s) and not of MDPI and/or the editor(s). MDPI and/or the editor(s) disclaim responsibility for any injury to people or property resulting from any ideas, methods, instructions or products referred to in the content.